Proceedings of the ASME 2017 36th International Conference on Ocean, Offshore and Arctic Engineering
OMAE2017
June 25-30, 2017, Trondheim, Norway

OMAE2017-61625

MODELS AND METHODS FOR EFFICIENCY ESTIMATION OF A MARINE ELECTRIC POWER GRID

Torstein I. Bø
Eilif Pedersen
NTNU - Norwegian University of Science and Technology,
Department of Marine Technology
7491 Trondheim, Norway
Email: torstein.bo@ntnu.no

ABSTRACT

Diesel electric propulsion has become industry standard for many marine applications. Typically, a significant part of the operations of vessels with diesel electric propulsion is done with low loads on the motors and generators. However, the efficiency of a drive train is typically only calculated for full load conditions. This underestimates the losses during low load conditions. This article presents modeling methods for the electric drive train, which can be used to estimate the efficiencies, also at low load. The models are established with limited parameter sets, as detailed information about of the components are seldom available. This article compares the estimated efficiency of the generator and motor with the given data from datasheets.

1 Introduction

During the last decade, many new topologies for diesel electric propulsion systems for marine vessels have been proposed. Diesel electric propulsion systems consists of multiple generator sets, which produce electric power. This power is distributed to the propulsion systems to propel the vessel, and other consumers such as winches, cranes, heave compensators, HVAC, and hotel loads. This is commonly used for vessels with varying propulsion demand or when high redundancy level is needed.

The fuel consumption of a marine vessel is often calculated when a new design is evaluated. This is typically done using a fuel consumption curve for the diesel engine while the efficiency of the electric system is assumed constant at its rated efficiency. However, for some vessels, such as platform supply vessels, the power demand may be low (typically below 15 % load of rated power) in a significant portion of the operational profile. This article presents models of the electric drive train, which can be used to model its efficiency. The presented model is developed for a DC distribution system; however, the models can be used as well for AC distribution with generators and variable speed drives based on voltage source inverters.

With DC distribution, the AC power from the synchronous generators are rectified to DC. A common DC bus is used to redistribute the power to the inverters, which converts the power to AC for propulsion motors or other loads. The DC bus may also be connected to energy storage or other DC loads, this is typically done using a DC/DC converter to control the power or the performance of the equipment. Multiple vendors deliver DC distribution systems, such as ABB (Onboard DC grid) [1], Siemens (BlueDrive plusC) [2], and Norwegian Electric Systems (Odin's Eye) [3]. Advantages and disadvantages of DC distribution compared with AC distribution are discussed in [4, 5].

Multiple models have been earlier developed to investigate the performance of marine power plants. The Italian Integrated Power Plant Ship Simulator models the electric system [6]. Marine Cybernetic's CyberSea is used for Hardware-in-the-Loop testing of marine power management systems [7]. In [8], a model of a naval vessel's DC power plant is presented. Marine Vessel and Power Plant System Simulator combines models of

the power plant, propulsion, hydrodynamics, and station keeping systems [9]. In [10], efficiencies for a voltage source inverter and induction motor are presented. Loss models based on equivalent circuits of induction motor and inverter are presented in [11]. A model of a DC power plant is presented in [12].

Hybrid series electric vehicles are the automotive equivalent of a diesel electric vessel. A model of such drive trains are presented in [13]. A study of the efficiency of this drive train is presented in [14], where the efficiency of the power electronics is fixed and the efficiency of the generator set and motor is approximated by polynomial functions. Multiple tools are developed for studies of vehicle's drive train such as ADVISOR [15], V-Elph [16], and PSIM [17].

The main contributions of this paper are models for generator and motors at diesel electric power plants and methods to estimate the needed parameters from limited parameter sets of the generator and motor. Multiple loss models are tested by splitting the given efficiency ratings into a training set for regression and an evaluation set. A model of ABB's, MARINTEK's, and NTNU's joint hybrid power lab is used to illustrate the method and to indicate the accuracy of the method.

The present article consists of two parts. The first part presents the models and a method to calculate parameters from available datasheets and catalog data. The second part evaluates the efficiencies of the different components and the total system. Conclusions are later drawn in Section 10. Details of the synchronous generator model are included in the appendix.

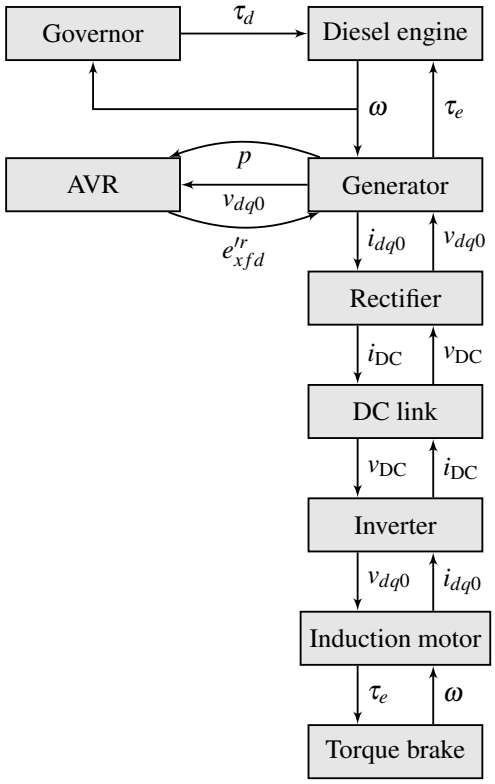

FIGURE 1. Topology of the plant.

2 Nomenclature

τ_d	Desired torque
τ_e	Electric torque
ω	Rotational speed
ψ	Magnetic flux linkage
e'^r_{xfd}	Field excitation voltage
$i_{dq0} = \begin{bmatrix} i_d & i_q & i_0 \end{bmatrix}^\top$	AC current in dq0-frame
i_{DC}	DC current
p	Active power
$v_{dq0} = \begin{bmatrix} v_d & v_q & v_0 \end{bmatrix}^\top$	AC voltage in dq0-frame
v_{DC}	DC voltage

3 Overview

The modeled plant is shown in Figure 1. A diesel engine is used to produce power, it is controlled by a governor. The diesel engine drives a generator, which produce electric power. The generator is controlled by an automatic voltage regulator (AVR). The AC power is converted to DC by the rectifier. A DC link is used to connect the producers and consumers. An inverter is used to convert the DC power to variable frequency AC. This AC power is used by the induction motor to turn a propeller or other load.

At full load, the main losses from the generator shaft to the motors shaft are in the generator and motor [18]. The efficiency of the generator and motor is typically 95-97 %, while efficiency of the variable speed drive (rectifier, DC link, and inverter) is typically 98-99 %. We will only model the losses of the generator and motor as these includes the major losses.

4 Generator

The generator is a synchronous machine and is modeled by simulating the magnetic flux linkage. The model is based on [19] and is included in the appendix. The model is chosen based on the parameters available from the datasheet. Magnetic saturation is not include in the model, as multiple tests are required to model the saturation profile. The parameters given in the datasheet are presented in Table 1. The data is given as standard synchronous machine reactances and standard synchronous machine time constants. These are converted to impedances by equations presented in [19, Ch. 7.4-7.5]. The primary damping wire in q-direction is neglected as typically done, since X'_q is not given in the datasheet.

TABLE 1. Data from datasheet of the synchronous generator. Impedance is given in per unit values.

Power	230 kVA	Voltage	450 V
Power factor	0.90	Frequency	50 Hz
Poles	4		
X_{ls}	0.150	X_{md}	6.390
X_{mq}	2.801	X'_{lfd}	6.6719
X'_{lkd}	0.2781	X'_{lkq2}	0.1385
r_s	0.0276	r'_{fd}	0.0061
r'_{kd}	0.3019	r'_{kq2}	0.0739

TABLE 2. Efficiency at full speed.

Power factor	Power			
	25 %	50 %	75 %	100 %
90 %	0.9297	0.9421	0.9376	0.9291
100 %	0.9380	0.9493	0.9452	0.9373

TABLE 3. Efficiency at 60 % speed.

Power factor	Power			
	15 %	30 %	45 %	60 %
90 %	0.9046	0.9347	0.9395	0.9378
100 %	0.9173	0.9450	0.9496	0.9483

TABLE 4. Candidate loss models.

	Loss model
1.	$a_1 + a_2\omega + a_3\psi$
2.	$a_1 + a_2\omega + a_3\psi + a_4\omega\psi$
3.	$a_1 + a_2\omega + a_3\omega^{1.5}\psi^{1.5}$
4.	$a_1 + a_2\omega + a_3\omega^2 + a_4\omega^{1.5}\psi^{1.5}$
5.	$a_1 + a_2\omega + a_3\omega^2 + a_4\omega\psi^2 + a_5\omega^2\psi^2 + a_6\omega^{1.5}\psi^{1.5}$

4.1 Loss model

The model from [19] only includes copper losses (ohmic losses); however, the iron and mechanical losses are significant. Table 4 shows five different candidate loss models, where $\psi = \sqrt{\left(\psi^r_{qs}\right)^2 + \left(\psi^r_{ds}\right)^2}$. The iron losses in an element can be modeled as [20]:

$$p_{\text{loss, magnetic}} = k_H B^2_{\max}\omega + k_c B^2_{\max}\omega^2 + k_E B^{1.5}_{\max}\omega^{1.5} \quad (1)$$

where the terms corresponds to hysteresis, eddy-current, and excess losses, respectively. $B_{\max}$ is the peak flux density, and k_H, k_c, and k_E are constants. $B_{\max}$ can be found by a detailed model of the magnetic flux, this requires a high fidelity model. Instead, we assume that ψ increases with $B_{\max}$. This is the motivation for testing terms like $\omega\psi^2$, $\omega^2\psi^2$, and $\omega^{1.5}\psi^{1.5}$. The mechanical losses are often assumed to give a linear friction torque, which gives the quadratic losses $a_1\omega + a_2\omega^2$. In addition, some linear models are tested for completeness.

The efficiency of the generator is given for four different load levels, two power factors (90 % and 100 %), and two speeds (60 % and 100 %). This gives 16 different operational points ($4 \times 2 \times 2$), which are presented in Tables 2 and 3.

The number of datapoints for the loss model is low. The sensitivity of the loss model with respect to selection of data points is therefore evaluated. This is done by doing the following steps:

1. Draw 7 to 10 data points for the *training set* from Tables 2 and 3, the remaining point are put in the *evaluation set*.
2. Optimize the loss model for the training set, such that the root mean square (RMS) error is obtained for the losses.
3. Calculate the estimated efficiency for the points in the training and evaluation set based on the optimized loss model.

This is done for all of the loss models and repeated for all combinations of training sets. The resulting rms errors are plotted as a point cloud in Figure 2. Each point represents a calculated rms error from a given training set. The cross represents the mean rms error for the loss model for all of the sets. In general, the higher order models gives a small error for the training set. However, due to the small training sets, they suffer from overparameterization, which gives large errors for the evaluation set. It should be noted that only two speeds for the generator are used, this may be the reason for the poor performance of the higher order models for ω. Model 3, $a_1 + a_2\omega + a_3\omega^{1.5}\psi^{1.5}$, is further used in this paper, as it gives the lowest rms error for the evaluation set.

4.2 Governor and Diesel Engine

The diesel engine is modeled as a rotating mass where the torque is controlled by the governor. Conservative rate constraints are used on the fuel index to avoid soothing and incomplete combustion [9]. In an AC grid, the governor is used to control active power sharing. However, the active power sharing is given by the voltage in a DC grid and not the electric angle as in AC grids. The speed is therefore controlled by a rate constrained PID-controller, which gives the desired torque to the diesel mo-

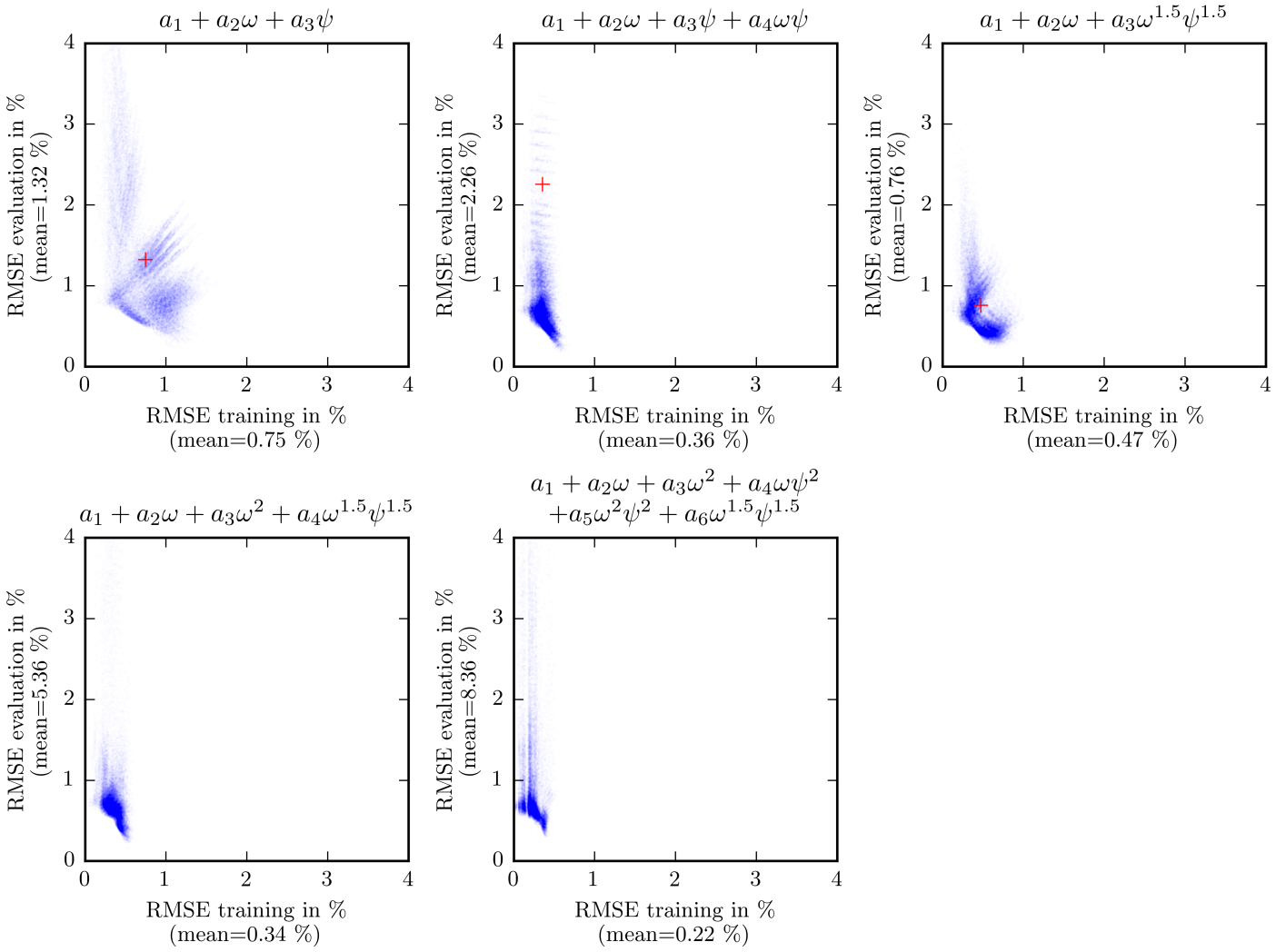

FIGURE 2. Root mean square error (RMSE) for the different loss models. Multiple training set is used to curve fit the loss model, which gives the minimum RMSE for the losses. The RMS error in the efficiency is plotted. The RMSE of the training set is plotted on the x-axis. The RMSE for the evaluation set is plotted on the y-axis. The cross shows the mean RMSE value.

tor:

$$\dot{\omega} = \frac{1}{I}(\tau_d - \tau_e - D\omega) \tag{2}$$

where ω is the diesel engine speed, I is the moment of inertia of the generator set, τ_d is the desired torque given by the governor, τ_e is the electric torque of the generator, and D is the linear damping coefficient.

4.3 AVR model

The automatic voltage regulator (AVR) is used to control the bus voltage and the active power sharing. Note that this differs from an AC plant where the AVR is used to control the reactive power sharing.

The set-point voltage is given by the droop curve, as seen in Figure 3. The voltage on the DC side on the rectifier is controlled by a PID controller, which gives the field voltage to the generator.

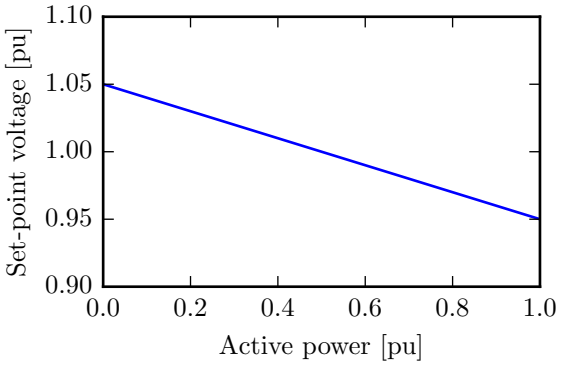

FIGURE 3. Droop curve of AVR

5 Rectifier

The rectifier is modeled as a transformer from AC to DC, with a fixed ratio between the AC voltage and the DC voltage. The model and parameters are adopted from [21]. However, the equations are rearranged to fit with the causality of the model:

$$i_{\mathrm{DC}} = k_i \sqrt{i_d^2 + i_q^2} \tag{3}$$

$$\delta = \arctan(\frac{i_d}{i_q}) - \phi \tag{4}$$

$$v_d = \frac{v_{\mathrm{DC}}}{k_v} \cos(\delta) \tag{5}$$

$$v_q = \frac{v_{\mathrm{DC}}}{k_v} \sin(\delta) \tag{6}$$

$$v_0 = 0 \tag{7}$$

These equations are valid when the generator is delivering power. The efficiency of the rectifier is $\eta = \frac{k_v k_i}{\cos\phi}$. The generator will start to consume power if the DC voltage is too high; however, this is nonphysically due to the thyristors in the rectifier. To avoid this v_{DC} is therefore modified:

$$v_{\mathrm{DC}} = \begin{cases} v_{\mathrm{DC,link}} & v_d i_d + v_q i_q > 0 \\ i_{\mathrm{DC}} R_{\mathrm{block}} & \text{otherwise} \end{cases} \tag{8}$$

where $v_{\mathrm{DC,link}}$ is the voltage at the common DC link. R_{block} block is a "blocking resistance" of the thyristor. It is not physical, but it is used to model the breaking property of a thyristor. R_{block} should be set to a high value to limit the nonphysical current.

6 DC link

The DC link is modeled as capacitor:

$$\dot{v}_{\mathrm{DC}} = \frac{1}{C} \sum i \tag{9}$$

where C is the capacitance of the DC-link including capacitance of filters connected to rectifiers and inverters. The current is positive when a component is delivering power and negative when consuming power.

7 Inverter

The inverter, which converts DC current to AC current, is modeled as a transformation from DC to AC with a constant efficiency. The inverter gets a frequency and voltage signal from the motor controller. An AC voltage signal is then generated and sent to the induction motor, the induction motor outputs a current. The DC voltage is given by the capacitor bank in the DC-link, a DC-current can therefore be calculated by power balance:

$$i_{\mathrm{DC}} = \frac{p}{v_{\mathrm{DC}} \eta} \tag{10}$$

Note that this model assumes fixed efficiency. The model is chosen as this is the only available data for the inverter. An alternative model is presented in [11] based on first principles; however, this model requires in-dept knowledge of the inverters IGBTs.

8 Induction Motor

The motor to test in this article is an ABB 400 V 4-pole 200 kW induction motor (M3BP 315 MLA 4). The available data for the motor is given in Table 5. A double-cage equivalent circuit model is used to model the motor, see Figure 4. The model and parameter estimation method is based on [22]. The resistance R_{ad} and R_{freg} are used to include all electric and magnetic losses in the model. The mechanical output of the motor is equal to the power through the resistance $R'_{21}\frac{1-s}{s}$ and $R'_{22}\frac{1-s}{s}$. The friction is assumed to be linear, hence, the mechanical losses $P_{\mathrm{mech,loss}} = D\omega^2$, this is not included in [22]. A resistance parallel to X_μ was included [22]; however, during the parameter optimization this resistance converged towards infinity in our study. Therefore, this resistance path is neglected.

The parameters are found by optimization. The cost function is a sum of the relative errors between the catalog values and the calculated values from the model. The parameters are optimized to minimize this cost function.

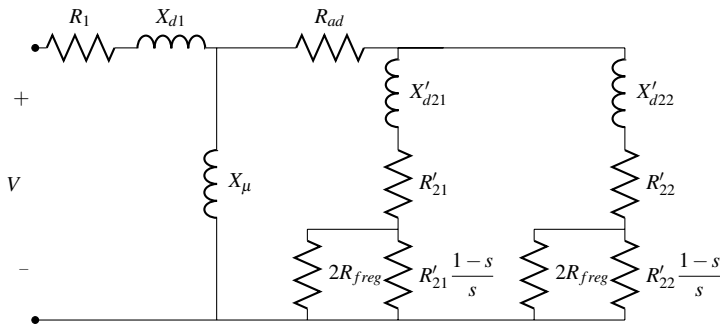

FIGURE 4. Equivalent circuit model of one phase of the induction motor.

The optimization problem is:

$$\begin{aligned} &\min_{\xi} e^\top e \\ &\text{subject to} \\ &0 \le \xi \end{aligned} \tag{11}$$

where $\xi = \left[R_1\ X_{d1}\ X_\mu\ R_{ad}\ X'_{d21}\ R'_{21}\ X'_{d22}\ R'_{22}\ R_{\text{freg}}\right]^\top$, $e = \frac{y - y_{\text{ref}}}{y_{\text{ref}}}$ and $y = \left[P_N\ \eta_{100\%}\ \eta_{75\%}\ \eta_{50\%}\ \text{pf}\ I_N\ I_S\ T_L\ T_B\right]$ which is the estimated values and y_{ref} is the catalog values. The details of the calculation of y is given in the appendix of [22].

The model is converted to dq0-reference frame through methods explained in [19, Ch. 3]. This removes the dependency between the phase angle and the states. It is the authors' experience that the computational speed is increased by 50 – 100 % when transforming the equations from the abc-reference frame to dq0-reference frame. Note that this model is based on steady state assumptions; this means that the model is only valid for slowly varying loads. Each of the three phases are simulated separately. This means that interaction effects, due to mutual inductions, are not included. However, the models are suited for modeling the motor's efficiency.

9 Results

9.1 Generator Efficiency

Figures 5 and 6 show the efficiency of the generator calculated from the models. The efficiency is estimated by running the generator with the rectifier, which gives a constant power factor (99.4 %). From Figure 5 we see that the efficiency of the generator set is mainly dependent on the power. The efficiency is independent of the speed in the loss model. It should be noted that the performance data is calculated values, as often is the case. It was expected that the losses increase with the increasing speed, as the friction losses and magnetic losses are increasing with increasing speed. In Figure 6, the efficiency from the datasheet is plotted for the generator at unity power factor. It seems plausible that the efficiency given by the datasheet is independent of the speed. This may be the source of the speed independence of the models. This highlights that a model based on parameters from a calculated datasheet (not experimentally validated) cannot be better than the model used to calculate the parameters in the datasheet. However, a system designer is often limited to such parameter set.

From the training of the loss model it was expected that the loss model is accurate within 1 %. In Figure 6, it is seen that the modeled efficiency is within 0.5 % from the efficiency given by the datasheet. Note that the efficiency is close to constant as long as the power is above approximately 20 %. Figure 6 plots the efficiency of the generator at rated speed.

It should be noted that the modeled generator is small, only 230 kVA. Generator sets used in marine vessels are typically of multiple MVA. Therefore, the efficiency is lower than what is normally expected, as the efficiency typically increases with the size of the generator. However, the modeling method is independent of the size of the generator.

TABLE 5. Data given for the induction motor

Power P_N	200 kW
Poles	4
Voltage	400 V
Speed	1486 rpm
$\eta_{100\%}$	95.6%
$\eta_{75\%}$	95.6%
$\eta_{50\%}$	95.3%
Power factor, pf	0.86
Nominal current I_N	351 A
Starting current $\frac{I_S}{I_N}$	7.2
Nominal torque T_N	1285 Nm
Locked rotor torque $\frac{T_L}{T_N}$	2.5
Breakdown torque $\frac{T_B}{T_N}$	2.9

9.2 Motor Efficiency

The induction motor efficiency is estimated by adjusting the voltage and frequency of the inverter and modifying the mechanical load. The voltage-frequency ratio is kept constant to achieve constant flux. Figures 7 and 8 show the efficiency of the induction motor. The estimated efficiency hits the efficiency given by

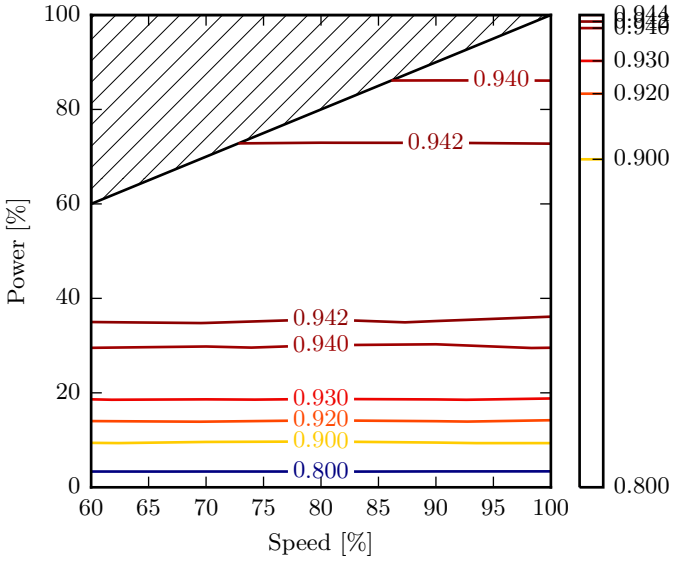

FIGURE 5. Efficiency of generator. Note that the contour lines are not equidistant. The shaded area is above the torque limit of the generator set.

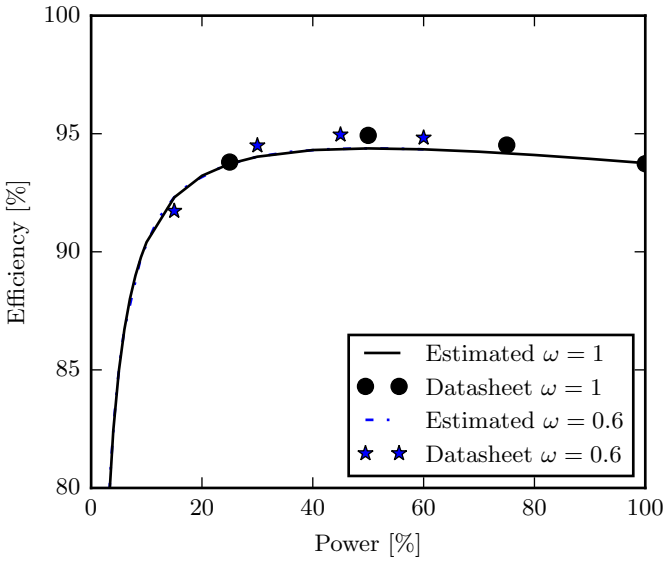

FIGURE 6. Estimated efficiency of generator, compared with efficiencies given by the datasheet.

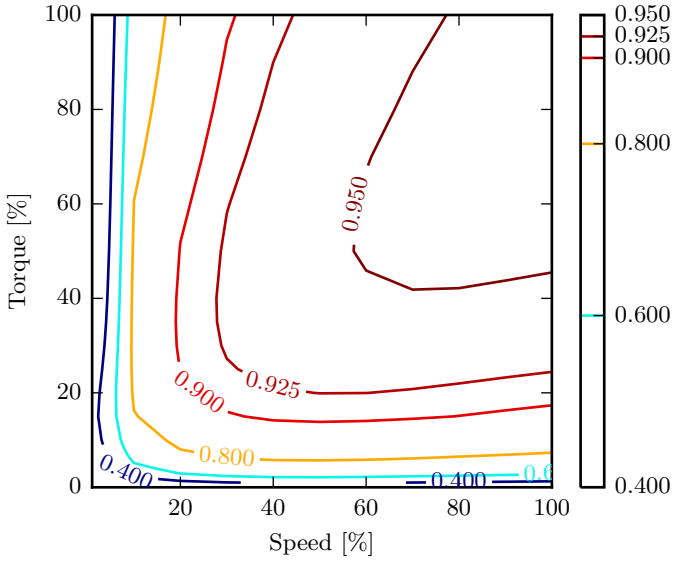

FIGURE 7. Efficiency of induction motor. Note that the contour lines are not equidistant.

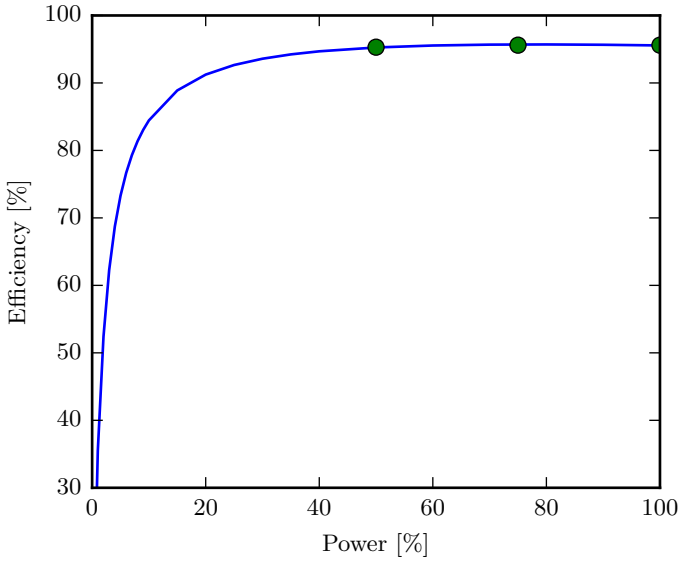

FIGURE 8. Estimated efficiency of induction motor at rated speed. The dots show the given efficiencies from the catalog.

the catalog values, as expected since the model is fitted for these values. Note that at rated speed the efficiency is approximately 95 % for loads higher than 40 %. The modeled induction motors are also small compared with normally used motors in marine applications, which gives lower efficiency than what could be expected. Again, the modeling method is independent of the size of the motor.

9.3 Combined Efficiency

The last figures are the combined efficiency, including the generator and motor efficiency. In this case, the generator and motor runs with the same relative load (when compared with

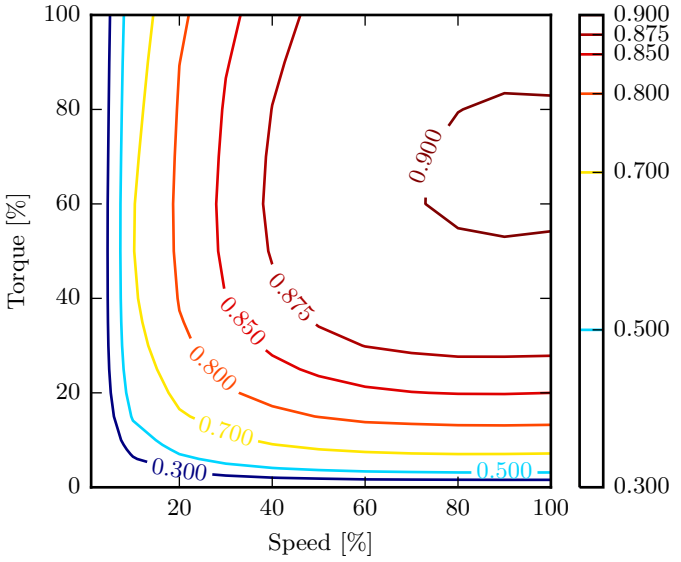

FIGURE 9. Efficiency of generator and induction motor combined. Note that the contour lines are not equidistant. The load level is assumed to be similar on both equipment. The generator set is assumed to run at its rated speed, as the efficiency is only weakly dependent on the speed.

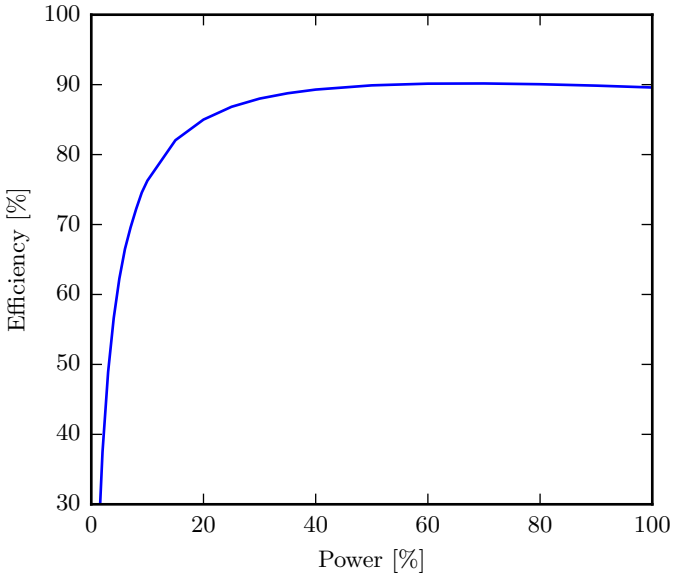

FIGURE 10. Efficiency of generator and induction motor combined. The load level is assumed to be similar on both equipment. The speed is set to the rated speed.

their rated power). The speed of the generator is kept at its optimal speed for the given load. The efficiency is shown in Figures 9 and 10. Note that the highest efficiency is around 90 % and the efficiency at lower speed quite low.

10 Conclusion

Simple methods are derived for loss modeling of electric machines. These models are based on catalog and datasheets values, which may be available for the propulsion plant designer. The designer can therefore use these models to increase the accuracy of estimated efficiency at off design conditions for the equipment.

Multiple loss models are evaluated for the synchronous generator. The data set is split such that one part of the parameters can be used for curve fitting, while the remaining set is used to evaluate the loss model. The best model estimates the efficiency within 1 % accuracy. However, the accuracy of the models are limited by the accuracy of the datasheet. For the induction model an establish method is used. Further work consist of verifying the models using experimental measurements from the lab.

REFERENCES

[1] J. F. Hansen, J. O. Lindtjørn, K. Vanska, Onboard DC Grid for enhanced DP operation in ships, in: Dynamic Positioning Conference, 2011.

[2] Siemens, New diesel electric propulsion system - BLUEDRIVE PlusC^{TM}.
URL http://w3.siemens.no/home/no/no/sector/industry/marine/pages/newdieselelectricpropulsionsystem.aspx

[3] Norwegian electric systems, Odin's eye® - dc grid solution (July 2016).
URL http://www.norwegianelectric.com/?menu=4&id=284

[4] J. G. Ciezki, R. W. Ashton, Selection and stability issues associated with a navy shipboard DC Zonal Electric Distribution System, IEEE Transactions on Power Delivery 15 (2) (2000) 665–669. doi:10.1109/61.853002.

[5] E. Skjong, R. Volden, E. Rodskar, M. Molinas, T. Johansen, J. Cunningham, Past, Present and Future Challenges of the Marine Vessel's Electrical Power System, IEEE Transactions on Transportation Electrification-doi:10.1109/TTE.2016.2552720.

[6] D. Bosich, M. Filippo, D. Giulivo, G. Sulligoi, A. Tessarolo, Thruster motor start-up transient in an all-electric cruise-liner: Numerical simulation and experimental assessment, Electrical Systems for Aircraft, Railway and Ship Propulsion, ESARSdoi:10.1109/ESARS.2012.6387447.

[7] T. Johansen, A. Sørensen, Experiences with HIL simulator testing of power management systems, in: Marine Technology Society, Dynamic Positioning Conference, 2009.

[8] M. Steurer, M. Andrus, J. Langston, L. Qi, S. Suryanarayanan, S. Woodruff, P. Ribeiro, Investigating the

Impact of Pulsed Power Charging Demands on Shipboard Power Quality, in: 2007 IEEE Electric Ship Technologies Symposium, IEEE, 2007, pp. 315–321. doi:10.1109/ESTS.2007.372104.

[9] T. I. Bø, A. R. Dahl, T. A. Johansen, E. Mathiesen, M. R. Miyazaki, E. Pedersen, R. Skjetne, A. J. Sørensen, L. Thorat, K. K. Yum, Marine Vessel and Power Plant System Simulator, IEEE Access 3 (2015) 2065–2079. doi:10.1109/ACCESS.2015.2496122.

[10] J. O. Estima, A. J. Marques Cardoso, Efficiency analysis of drive train topologies applied to electric/hybrid vehicles, IEEE Transactions on Vehicular Technology 61 (3) (2012) 1021–1031. doi:10.1109/TVT.2012.2186993.

[11] S. S. Williamson, A. Emadi, K. Rajashekara, Comprehensive Efficiency Modeling of Electric Traction Motor Drives for Hybrid Electric Vehicle Propulsion Applications, IEEE Transactions on Vehicular Technology 56 (4) (2007) 1561–1572. doi:10.1109/TVT.2007.896967.

[12] C. L. Su, K. L. Lin, C. J. Chen, Power flow and generator-converter schemes studies in ship MVDC distribution systems, IEEE Transactions on Industry Applications 2015 (1) (2015) 50–59. doi:10.1109/TIA.2015.2463795.

[13] S. Bogosyan, M. Gokasan, D. Goering, A Novel Model Validation and Estimation Approach for Hybrid Serial Electric Vehicles, IEEE Transactions on Vehicular Technology 56 (4) (2007) 1485–1497. doi:10.1109/TVT.2007.899340.

[14] X. Hu, N. Murgovski, L. Johannesson, B. Egardt, Energy efficiency analysis of a series plug-in hybrid electric bus with different energy management strategies and battery sizes, Applied Energy 111 (2013) 1001–1009. doi:10.1016/j.apenergy.2013.06.056.

[15] T. Markel, A. Brooker, T. Hendricks, V. Johnson, K. Kelly, B. Kramer, M. O'Keefe, S. Sprik, K. Wipke, ADVISOR: A systems analysis tool for advanced vehicle modeling, Journal of Power Sources 110 (2) (2002) 255–266. doi:10.1016/S0378-7753(02)00189-1.

[16] K. Butler, M. Ehsani, P. Kamath, A Matlab-based modeling and simulation package for electric and hybrid electric vehicle design, IEEE Transactions on Vehicular Technology 48 (6) (1999) 1770–1778. doi:10.1109/25.806769.

[17] S. Onoda, A. Emadi, PSIM-Based Modeling of Automotive Power Systems: Conventional, Electric, and Hybrid Electric Vehicles, IEEE Transactions on Vehicular Technology 53 (2) (2004) 390–400. doi:10.1109/TVT.2004.823500.

[18] A. K. Ådnanes, Maritime Electrical Installations and Diesel Electric Propulsion, Oslo, Norway, 2003.

[19] P. C. Krause, O. Wasynczuk, S. D. Sudhoff, Analysis of Electric Machinery and Drive Systems, 2nd Edition, McGraw Hill Higher Education, 2002.

[20] M. Ranlöf, A. Wolfbrandt, J. Lidenholm, U. Lundin, Core loss prediction in large hydropower generators: Influence of rotational fields, IEEE Transactions on Magnetics 45 (8) (2009) 3200–3206. doi:10.1109/TMAG.2009.2019115.

[21] I. Jadric, D. Borojevic, M. Jadric, Modeling and control of a synchronous generator with an active DC load, IEEE Transactions on Power Electronics 15 (2) (2000) 303–311. doi:10.1109/63.838103.

[22] M. Torrent, Estimation of equivalent circuits for induction motors in steady state including mechanical and stray load losses, European Transactions on Electrical Power 22 (7) (2012) 989–1015. doi:10.1002/etep.621.

APPENDIX: Generator model

The equations for the generator model is adopted from [19]. See [19] for definitions of the variables and parameters.

$$\dot{\psi}^r_{qs} = \omega_b \left[v^r_{qs} - \frac{\omega_r}{\omega_b}\psi^r_{ds} + \frac{r_s}{X_{ls}}\left(\psi^r_{mq} - \psi^r_{qs}\right)\right] \tag{12}$$

$$\dot{\psi}^r_{ds} = \omega_b \left[v^r_{ds} + \frac{\omega_r}{\omega_b}\psi^r_{qs} + \frac{r_s}{X_{ls}}\left(\psi^r_{md} - \psi^r_{ds}\right)\right] \tag{13}$$

$$\dot{\psi}^r_{0s} = \omega_b \left[v^r_{qs} - \frac{r_s}{X_{ls}}\psi^r_{0s}\right] \tag{14}$$

$$\dot{\psi}'^r_{kq2} = \omega_b \left[v'^r_{kq2} + \frac{r'_{kq2}}{X'_{lkq2}}\left(\psi^r_{mq} - \psi'^r_{kq2}\right)\right] \tag{15}$$

$$\dot{\psi}'^r_{fd} = \omega_b \left[\frac{r'_{fd}}{X_{md}} e'^r_{xfd} + \frac{r'_{fd}}{X'_{lfd}}\left(\psi^r_{md} - \psi'^r_{fd}\right)\right] \tag{16}$$

$$\dot{\psi}'^r_{kd} = \omega_b \left[v'^r_{kd} + \frac{r'_{kd}}{X'_{lkd}}\left(\psi^r_{md} - \psi'^r_{kd}\right)\right] \tag{17}$$

It is assumed that the damping wires are short circuited; hence, $v'^r_{kq2} = v'^r_{kd} = 0$.

$$i^r_{qs} = -\frac{1}{X_{ls}}\left(\psi^r_{qs} - \psi^r_{mq}\right) \tag{18}$$

$$i^r_{ds} = -\frac{1}{X_{ls}}\left(\psi^r_{ds} - \psi^r_{md}\right) \tag{19}$$

$$i^r_{0s} = -\frac{1}{X_{ls}}\psi^r_{0s} \tag{20}$$

$$i'^r_{kq2} = \frac{1}{X'_{lkq2}}\left(\psi'^r_{kq2} - \psi^r_{mq}\right) \tag{21}$$

$$i'^r_{fd} = \frac{1}{X'_{lfd}}\left(\psi'^r_{fd} - \psi^r_{md}\right) \tag{22}$$

$$i'^r_{kd} = \frac{1}{X'_{lkd}}\left(\psi'^r_{kd} - \psi^r_{md}\right) \tag{23}$$